SAE TECHNICAL PAPER SERIES

2002-01-1088

Axial Flux Variable Gap Motor: Application in Vehicle Systems

Sung Chul Oh, Justin Kern, Ted Bohn, Aymeric Rousseau and Maxime Pasquier
Argonne National Laboratory

Reprinted From: Advanced Hybrid Vehicle Powertrain Technology (SP–1697)

The Engineering Society For Advancing Mobility Land Sea Air and Space®
INTERNATIONAL

SAE 2002 World Congress
Detroit, Michigan
March 4-7, 2002

ISSN 0148-7191

Printed in USA

2002-01-1088

Axial Flux Variable Gap Motor: Application in Vehicle Systems

Sung Chul Oh, Justin Kern, Ted Bohn, Aymeric Rousseau and Maxime Pasquier
Argonne National Laboratory

ABSTRACT

Alternative electric motor geometry with potentially increased efficiency is being considered for hybrid electric vehicle applications. An axial flux motor with a dynamically adjustable air gap (i.e., mechanical field weakening) has been tested, analyzed, and modeled for use in a vehicle simulation tool at Argonne National Laboratory. The advantage of adjusting the flux is that the motor torque-speed characteristics can better match the vehicle load. The challenge in implementing an electric machine with these qualities is to develop a control strategy that takes advantage of the available efficiency improvements without using excessive energy to mechanically adjust the air gap and thus reduce the potential energy savings. Motor efficiency was mapped in terms of speed, torque, supply voltage, and rotor-to-stator air gap. Maps of optimal gap versus efficiency were used to develop a motor model and control strategy, which were incorporated into the PNGV Systems Analysis Toolkit vehicle modeling software.

INTRODUCTION

Axial flux geometry, in which the machine is made from two opposing disks — one fixed and one rotating — has two substantial advantages over radial flux geometry, in which a drum rotates inside a cylinder. First, there are significant volume savings over the more commonly used radial flux geometry, for which much of the internal volume of the rotor does not contribute to power output. Second, and more importantly, axial flux geometry allows a very simple technique for field weakening that relies on mechanical adjustment of the air gap, which does not impinge significantly on efficiency. Within a reasonable band, increasing the air gap increases the copper loss as the torque constant decreases, but decreases the iron loss as the flux density is reduced [1]. Motor air gap is a key design parameter in any motor design that directly affects the motor torque output and back electromotive force (EMF) constant. In a conventional radial flux motor, the air gap is optimized for a single motor torque-speed operating point. Therefore, at off-design-point motor torque, speed and resulting efficiency are not optimized. The axial flux motor allows the possibility of actively varying the rotor-to-stator air gap to optimize the motor performance and efficiency for a particular operating point. So far, axial flux motors are mainly used in high- torque, low-speed applications because of its inherent characteristics. The model investigated here was used in solar cars as a direct-drive propulsion system [2]. Recently, use of an axial flux motor for the starter/alternator has been proposed [3].

For this experiment, we measured the efficiency at distinct operating points (torque, speed, input voltage, and air gap) in all four quadrants of operation (forward powering, forward regeneration, reverse powering, reverse regeneration). Measured results were analyzed to determine the air gap, which optimizes efficiency at a given torque, speed, and input voltage. Also vehicle performance was simulated with the PNGV Systems Analysis Toolkit (PSAT) vehicle modeling software based on the motor test results.

MOTOR SPECIFICATIONS

There are several torque and power curves that are of interest when evaluating a traction drive motor [4]:

- Electrical peak torque and power, which are limited by electrical characteristics of the motor (i.e., pull-out torque);
- Current limited peak torque and power, which are limited by the maximum design current of the inverter;
- Motor thermal limited torque and power, which are limited by the time it takes the stator and/or rotor to increase from the rated cooling temperature to the maximum design temperature; and
- Motor thermal limited continuous torque and power, which are limited by the amount of heat

the motor can reject when in thermal equilibrium.

In most cases, the above specifications are provided by the manufacturers, and they can be verified by the experiment.

General specifications for the test motor, taken from the manufacturer's data sheet are listed in Table 1. This motor is designed and manufactured by New Generation Motor Corporation [5].

Table 1: Motor Specifications

Continuous Power (kW)	2.5
Rated Speed (rpm)	300
Rated Torque (Nm)	102
Rated Voltage (V)	48
Cooling	Air cooling
Min/Max Air Gap (mm)	1.8/6.0
Motor Diameter (mm)	315
Motor Width (mm)	70
Weight (kg)	20
Type	DC Brushless Permanent Magnet

TEST SETUP

The following equipment is needed to test four-quadrant operation of electric motors.

- Bi-directional DC power supply (battery simulator) — During powering and regeneration, current is provided in either direction (from source to motor, from motor to source).
- Active controlled load (dynamometer) — Speed and direction of load should be controlled according to the desired quadrant operation.
- Automatic data acquisition system

The test setup was assembled in Argonne's Advanced Powertrain Test Facility (APTF). A block diagram of the test setup according to the stated requirements is shown in Figure 1.

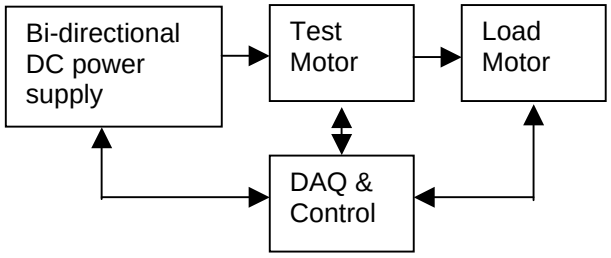

Figure 1: Block diagram of test setup

Figures 2 and 3 are photographs of the test setup. An axial flux motor was mounted onto the dynamometer on a portable test stand. For this experiment, the dynamometer only served as a through shaft and support bearings. The test motor was adapted via a coupling to the flange on one side of the dynamometer. An induction motor was also mounted on the portable test stand and coupled to the opposite side of the dynamometer via a flex coupling and a straight, flanged drive shaft. The test motor was controlled via a remotely located (control room) interface with the computer control.

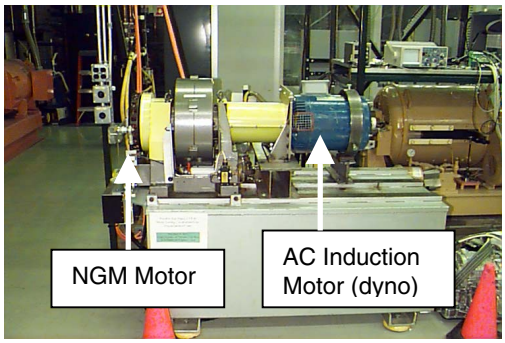

Figure 2: Portable Motor Test Stand

The test motor was powered by the motor controller via a DC feed directly from one channel of an ABC-150 DC power supply. The rotor-to-stator gap was changed manually by rotating a gear-driven lead screw or by servo motor between tests. Control of the induction motor was via an AC vector-drive motor controller. This motor was used as a load motor for either speed or torque control.

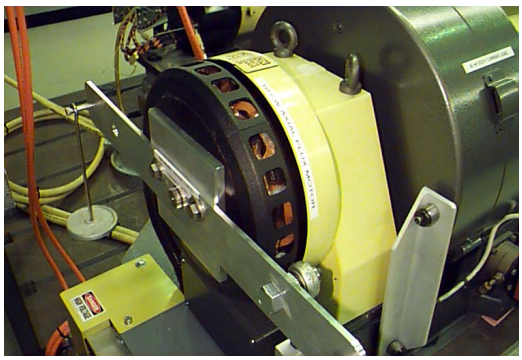

Figure 3: NGM Axial Gap Motor

TEST PROCEDURE

Four-quadrant motor operation is defined in Figure 4.

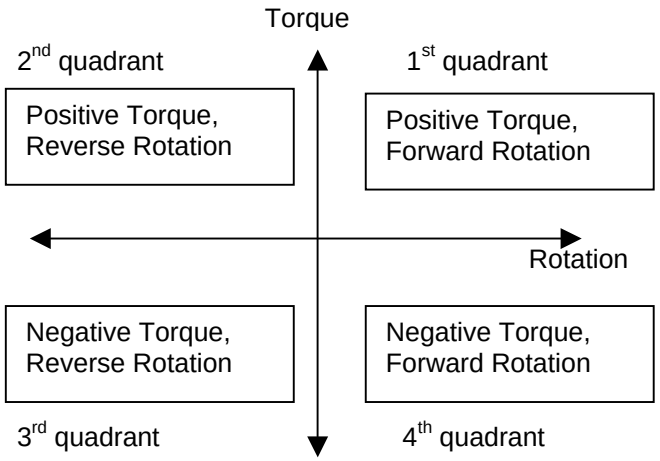

Figure 4: Definition of Operating Quadrants

The test motor and load motor should be operated as prescribed in Table 2 for each quadrant of operation.

Table 2: Operating Mode of Test and Load Motors

Motor mode: REGEN Motor direction: REV: 2nd Quad Load direction: REV	Motor mode: THROTTLE Motor direction: FWD: 1st Quad Load direction: FWD
Motor mode: THROTTLE Motor direction: REV: 3rd Quad Load direction: REV	Motor mode: REGEN Motor direction: FWD: 4th Quad Load direction: FWD

In the case of throttle mode, the test motor supplies torque to the load motor, and the energy flow is from DC source to test motor. During regeneration, the energy flow is from test motor to DC source by the mechanical input from the load motor. The following signals were measured to calculate motor efficiency. Efficiency during throttle mode is calculated as follows.

$$efficiency = \frac{motor\ torque \times motor\ speed}{DC\ input\ voltage \times DC\ input\ current}$$

Efficiency during regeneration mode is calculated as follows.

$$efficiency = \frac{DC\ input\ voltage \times DC\ input\ current}{motor\ torque \times motor\ speed}$$

- DC input current
- DC input voltage
- Motor torque
- Motor speed
- Motor temperature

The measured signals were collected with a Labview data-acquisition program. The test motor was operated in torque mode, and the load motor (induction motor) was operated in speed mode. The load motor was controlled to the desired speed, and then the torque from the test motor was increased to the desired torque. At that point, the above signals were measured and recorded, and the system efficiency was calculated. Peak toque and maximum speed were also measured.

TEST RESULTS

TORQUE-SPEED CURVE

Maximum torque at each air gap and operating speed was measured and recorded and is shown in Figure 5. To measure maximum torque, torque command was increased until output torque did not increase. Output torque at that point was defined as maximum torque. To measure maximum speed, speed command was increased until output torque reached zero. This speed was defined as maximum speed. As expected, maximum torque decreases as air gap increases and maximum speed increases as air gap increases. The maximum torques at the 5-mm and 6-mm air gaps were relatively close because of air gap measurement error. More precise air gap measurement is recommended.

By adjusting the air gap, the operating area of test motor can be extended. The maximum torque is 136 N-m at 400 rpm with an air gap of 1.5 mm and the maximum speed is 1,200 rpm with an air gap of 6 mm.

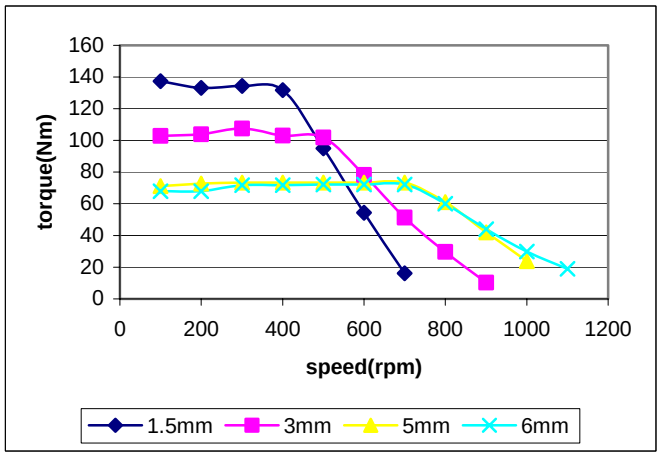

Figure 5: Maximum Torque Curve With Varying Air Gap

EFFICIENCY MAPS FOR DIFFERENT AIR GAPS

FIRST-QUADRANT OPERATION. Efficiencies at various speeds and torques at each air gap were measured and are shown in Figures 6 and 7. As shown in the figures, efficiency increases as speed increases. Efficiency increases as torque increases up to a certain value and then decreases. Efficiency near maximum torque is relatively low.

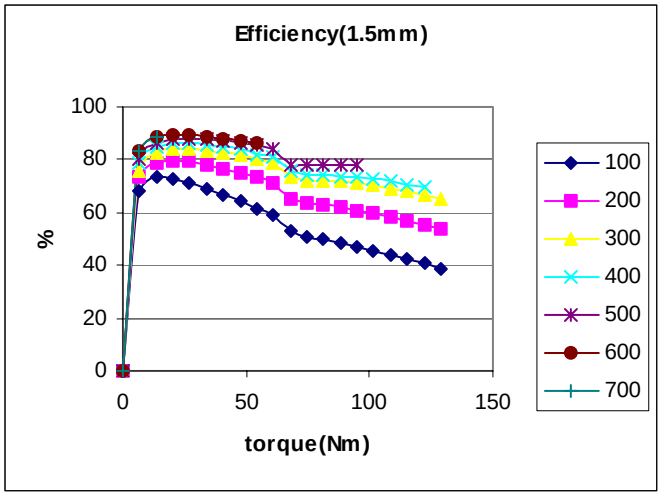

Figure 6: Efficiency at Different Speeds (1.5-mm gap)

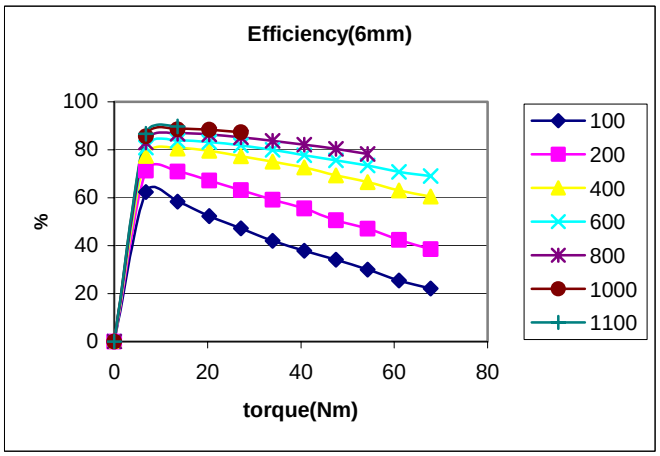

Figure 7: Efficiency at Different Speeds (6-mm air gap)

Efficiency decreases as the air gap increases, except in the low-torque region. In this region, efficiency can be improved by adjusting the air gap. This finding suggests that the optimal air gap that maximizes efficiency at the low-torque region can be obtained by interpolation.

OPTIMAL AIR GAP FOR DIFFERENT OPERATING POINTS

Based on the test results described above, we estimated the optimal air gap for different operating points (speed and torque). To determine the optimal air gap, power loss at specific points was measured at each air gap. Power loss was interpolated at intermediate points, and the minimum point was estimated on the basis of the interpolated result. Figure 8 shows the variation of power loss at each air gap. In the case of first-quadrant operation, power loss is defined as the difference between input electrical power (input dc voltage × input dc current) and output mechanical power (motor speed × torque). In most cases, power loss increases as air gap increases, except in the low-torque region. In this case, optimal air gap is defined as a point at which power loss is at a minimum. Power loss between measured points was interpolated based on measured data, and the minimum point was identified. In Figure 8, the optimal air gap is defined as 3.9 mm.

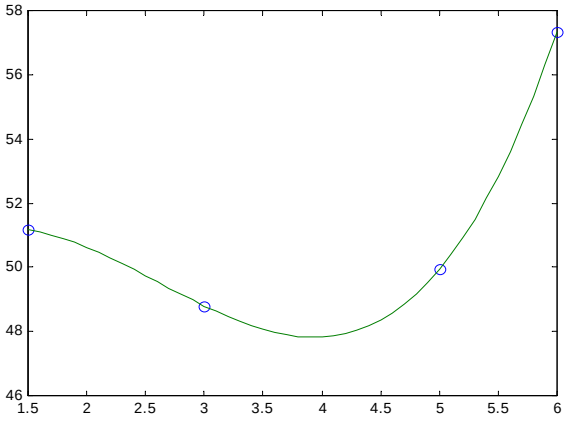

Figure 8: Power Loss Variation (200 rpm, 5 ft-lbs)

At light load, the stator flux may be saturated. In this case, by increasing the air gap, the stator flux can be reduced and flux-related losses — such as core loss — can also be reduced, which would improve the efficiency. But as torque increases, required flux also increases and the efficiency would not be improved by adjusting the air gap.

As shown in Figure 9, the optimal air gap increases as speed increases. Conversely, the optimal air gap at low torque is relatively large. In general, high efficiency can be obtained at middle to high speed and the low- to middle-torque region. Efficiency distribution is shown in Figure 10.

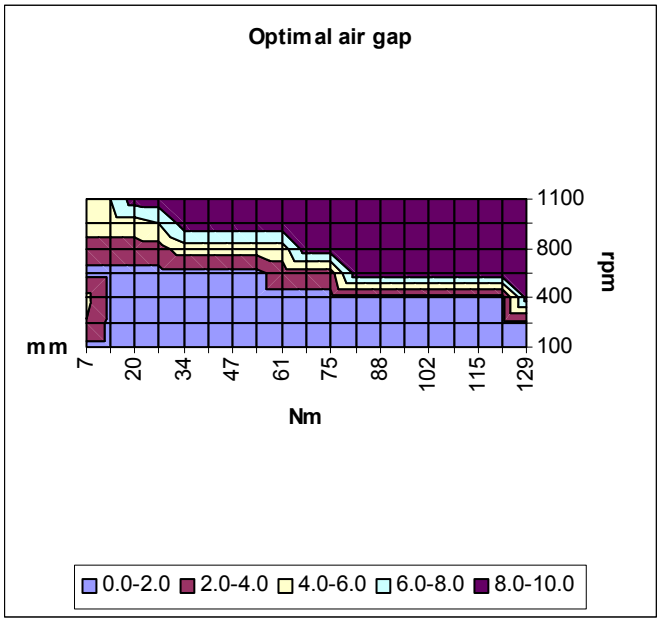

Figure 9: Optimal air gap

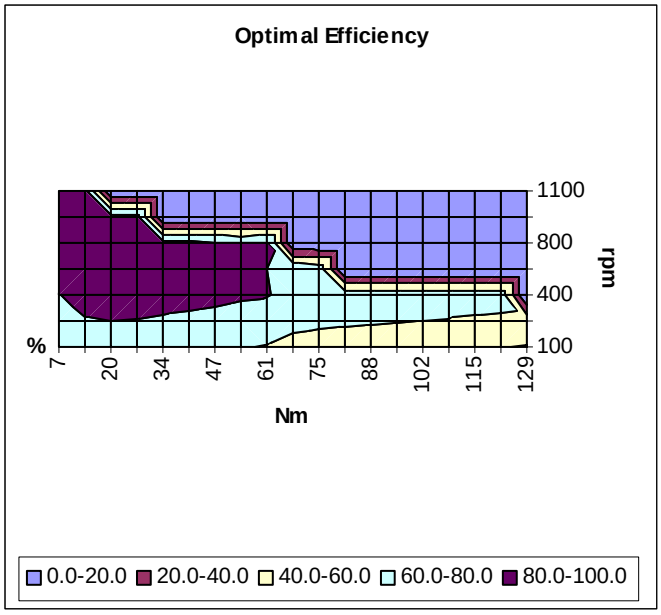

Figure 10: Optimal efficiency

(Note: 8-10mm and 0-20 % regions are non-operative)

EFFICIENCY MAPS FOR DIFFERENT OPERATING POINTS

FORWARD REGENERATION (FOURTH-QUADRANT OPERATION). Maximum torque at each speed and air gap was measured. As shown in Figure 11, the operating area for fourth quadrant operation is squarer than that of first quadrant operation and the maximum torque is reduced. (137 Nm => 89.5 Nm) The reason is that the regeneration region is restricted due to the back EMF of the motor.

This mode can occur during electrical braking. Braking torque decreases as air gap increases. Maximum speed at which regenerative braking is possible, increases as air gap increases. If this characteristic is considered into braking control strategy the overall efficiency can be improved. One of the possible control strategies is changing air gap according to the braking torque.

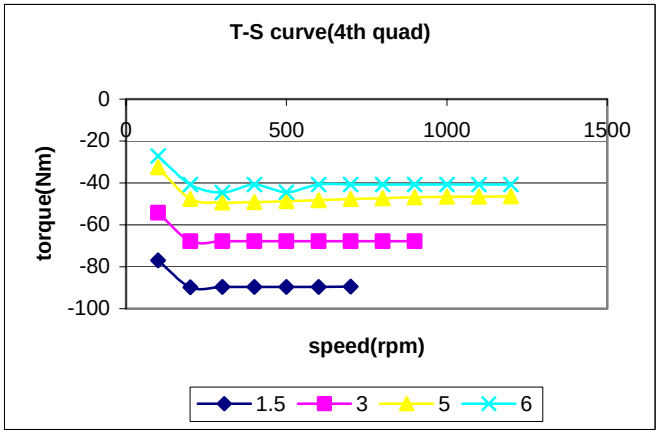

Figure 11: T-S Curve With Varying Air Gap

Efficiency is also measured for different operating points. During regeneration, efficiency is defined as ratio between mechanical input power and electrical output power. Efficiencies at different air gap are shown in figures 12 and 13.

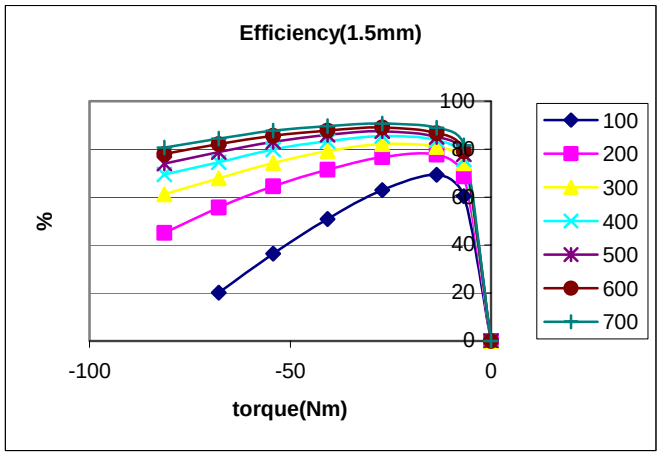

Figure 12: Efficiency at Different Speeds (1.5mm gap)

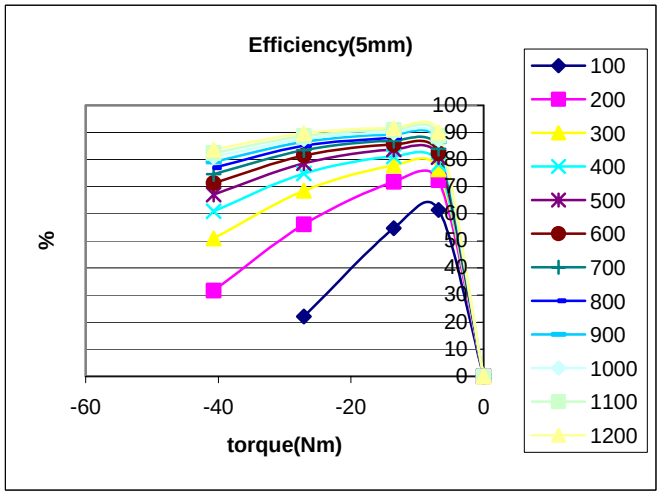

Figure 13: Efficiency at Different Speeds (5mm gap)

The optimal air gap is estimated by using the same method as was used for first-quadrant operation. The optimal air gap and efficiency distribution are shown in Figures 14 and 15, respectively.

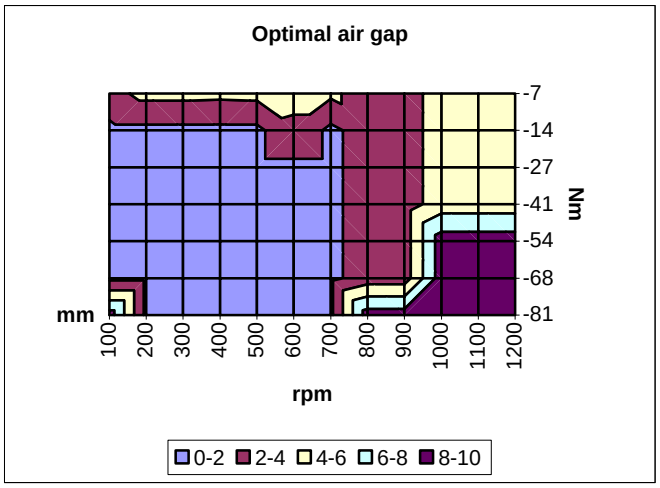

Figure 14: Optimal Air Gap

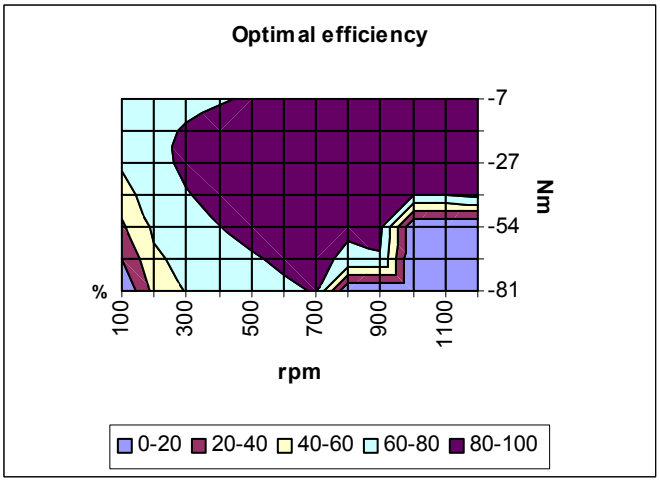

Figure 15: Optimal Efficiency

REVERSE POWERING (THIRD-QUADRANT OPERATION). The efficiency at each operating point was measured, and the optimal air gap with respect to efficiency was estimated for third-quadrant operation. The maximum torque at different air gaps is shown in Figure 16. The efficiency at a 3-mm air gap is shown in Figure 17. Overall characteristics are similar to those of first-quadrant operation.

The optimal air gap was estimated by using the same method as that used for first-quadrant operation. The optimal air gap and efficiency distribution are shown in Figures 18 and 19, respectively.

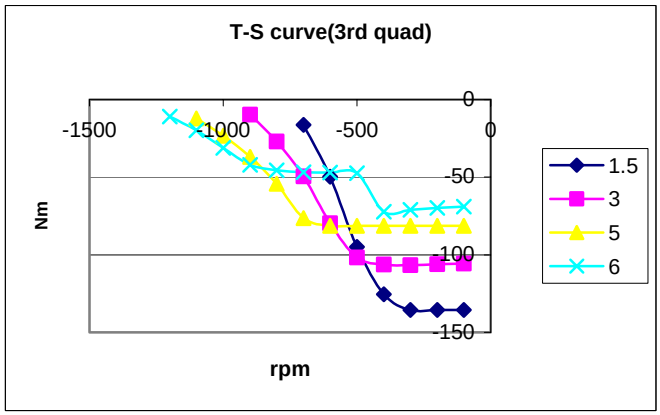

Figure 16: Maximum Torque

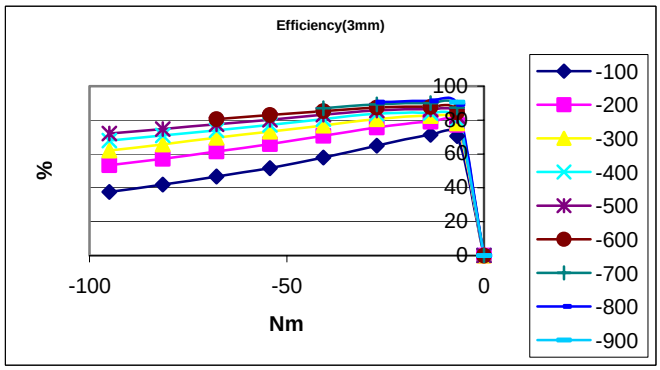

Figure 17: Efficiency (3 mm air gap)

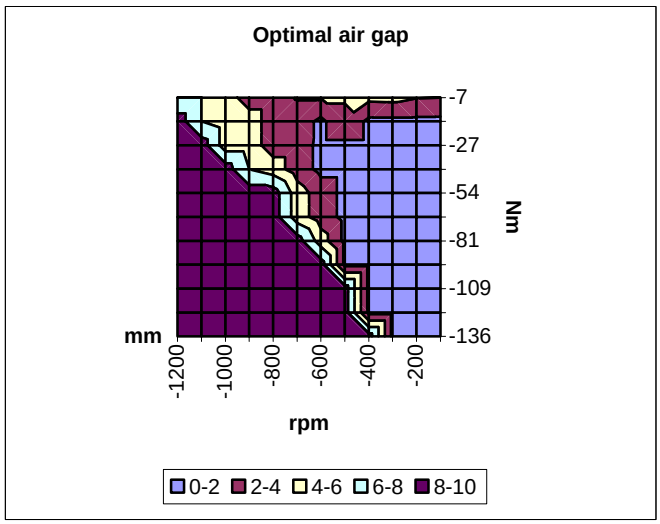

Figure 18: Optimal Air Gap

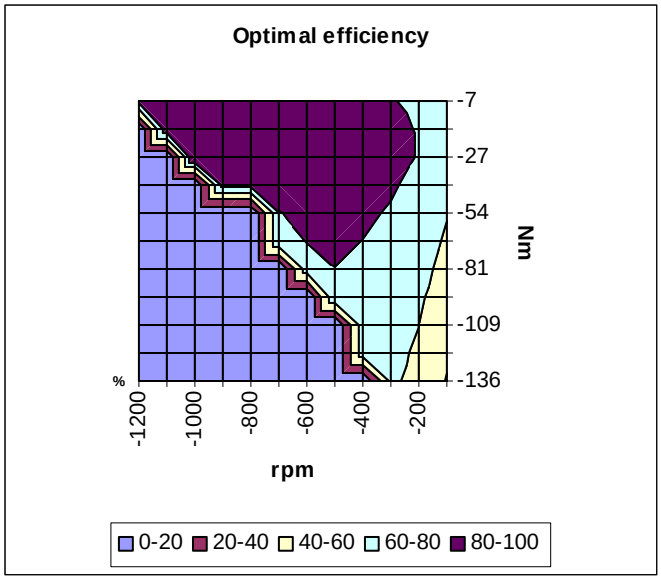

Figure 19: Optimal efficiency

REVERSE REGENERATION (SECOND-QUADRANT OPERATION). The efficiency at each operating point was measured, and the optimal air gap and efficiency were estimated. The maximum torque in second-quadrant operation is shown in Figure 20, and the efficiency at a 1.5-mm air gap is shown in Figure 21. Overall characteristics are similar to those of fourth-quadrant operation.

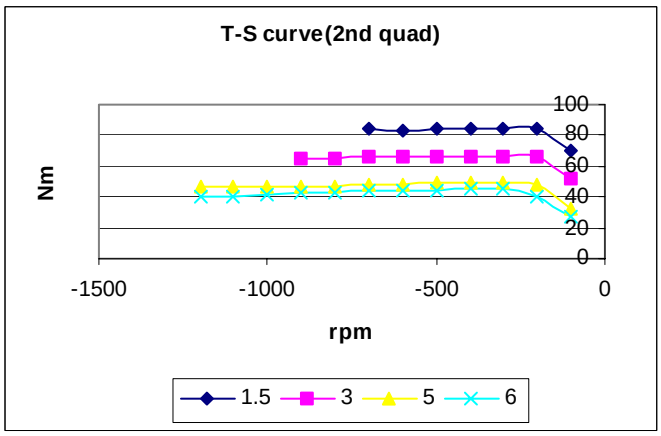

Figure 20: Maximum Torque With Varying Air Gap

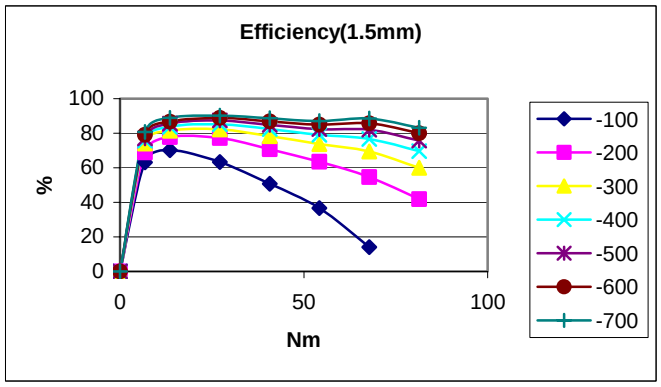

Figure 21: Efficiency at different speeds (1.5 mm gap)

The optimal air gap was estimated by using the same method as that used for first-quadrant operation. The optimal air gap and efficiency distribution are shown in Figures 22 and 23, respectively.

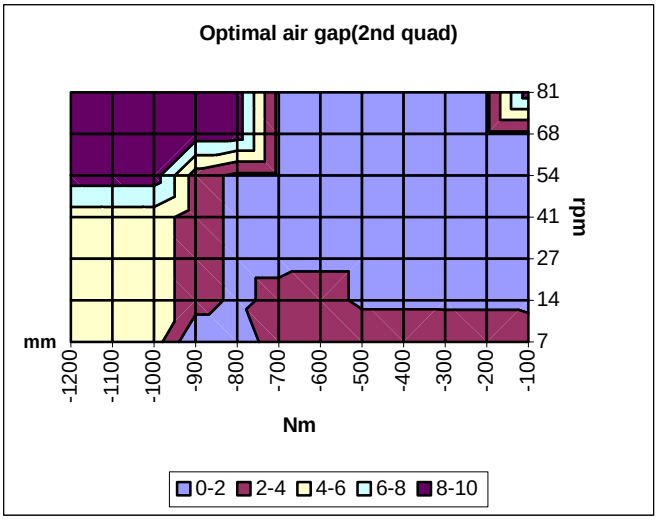

Figure 22: Optimal Efficiency

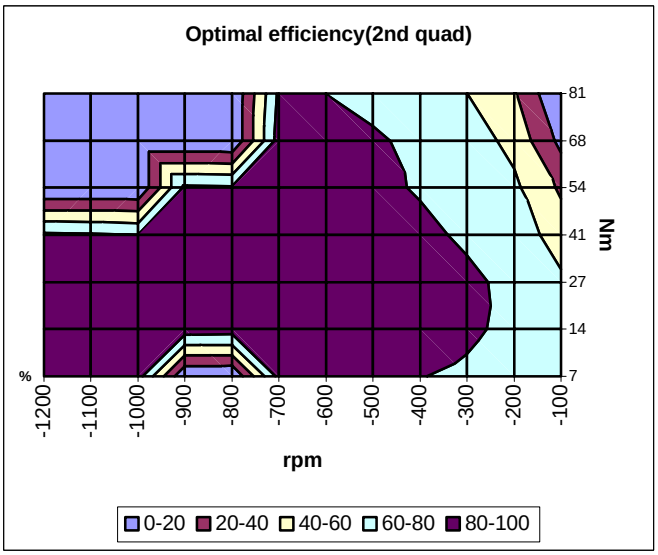

Figure 23: Optimal efficiency

OPTIMAL AIR GAP AND EFFICIENCY FOR FOUR-QUADRANT OPERATION. Figure 24 shows maximum torque for each quadrant of operation. The first and third quadrant characteristics are symmetrical, and the second and fourth quadrant characteristics are symmetrical.

The maximum torque of the first quadrant is larger than that of the second and fourth quadrants because the back EMF restricts the regeneration region. The maximum speed of the regeneration region is larger than that of the powering region. The regeneration regions (second and fourth quadrants) are much squarer than the powering regions (first and third quadrants). The characteristics of all four quadrants are essential to

improving overall vehicle efficiency. During braking and downhill coasting, the second- and fourth-quadrant characteristics should be considered to improve efficiency.

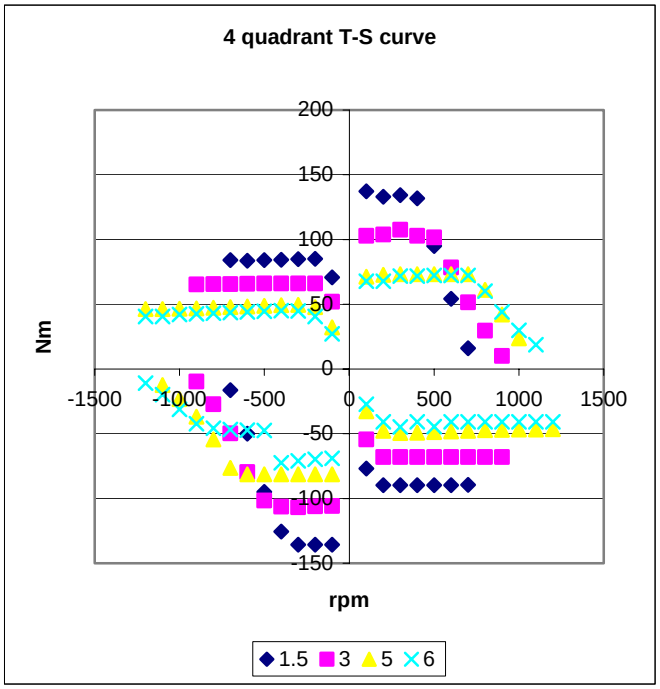

Figure 24: Maximum Torque in Four-Quadrant Operation

The optimal air gap and efficiency distribution for four-quadrant operation are shown in Figures 25 and 26, respectively.

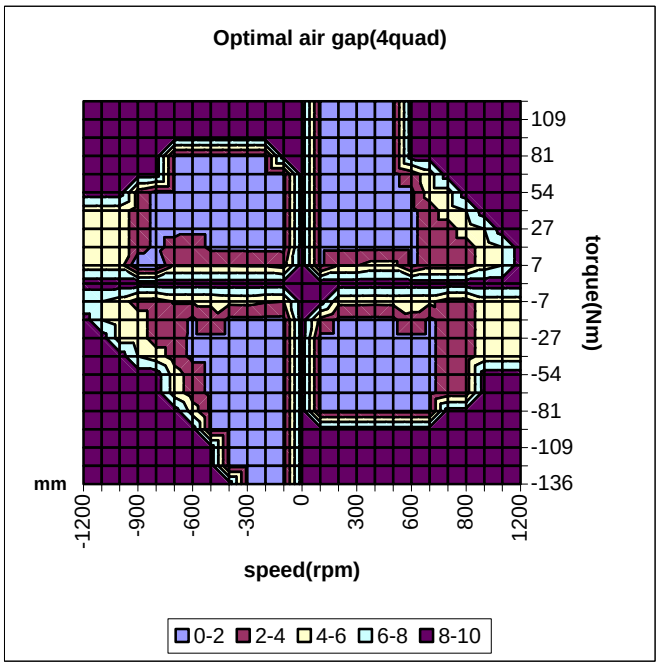

Figure 25: Optimal Air Gap (four-quadrant operation)

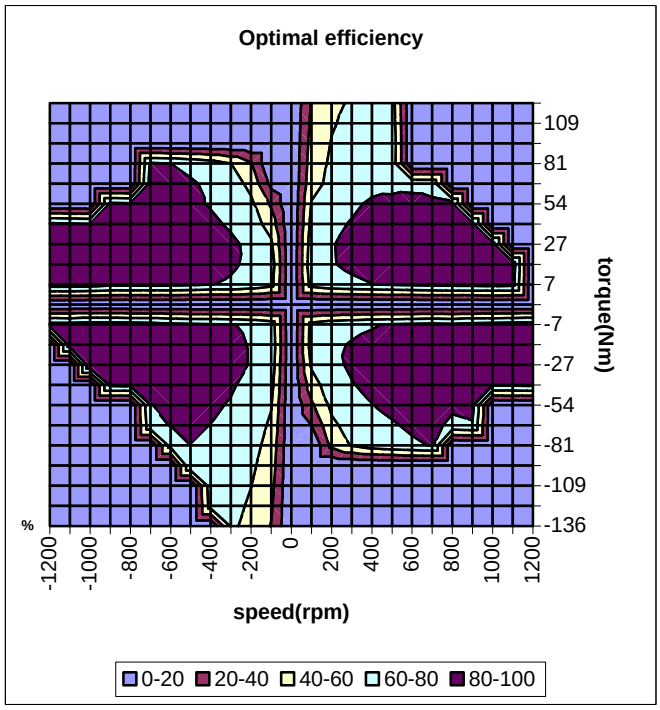

Figure 26: Optimal Efficiency (fourth quadrant)

TORQUE-SPEED CURVE FOR DIFFERENT INPUT VOLTAGES. If a battery is used as a power source for the motor, the buss voltage will vary during operation. To analyze the effect of input voltage variation, we measured the maximum torque and efficiency at each input voltage. The maximum torque variations at different voltages and different air gaps are shown in Figures 27, 28, 29, and 30.

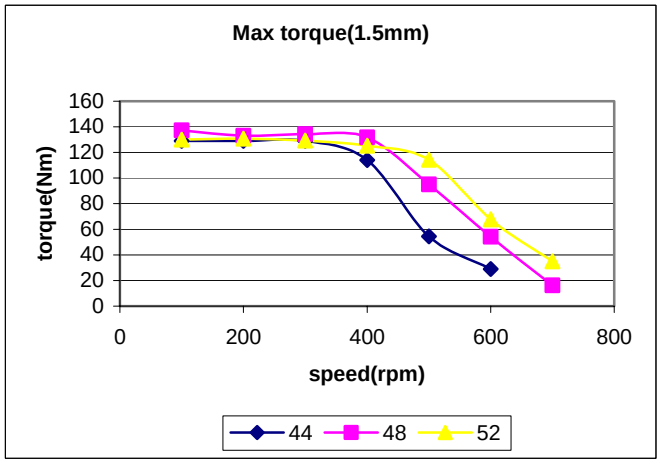

Figure 27: Maximum Torque at Different Input Voltages (1.5-mm gap)

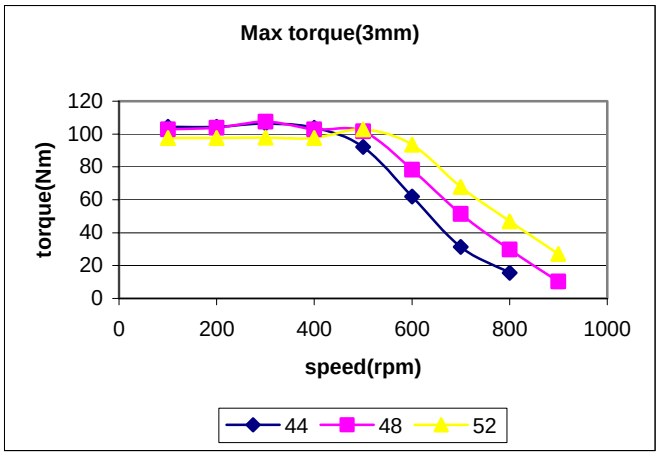

Figure 28: Maximum Torque at Different Input Voltages (3-mm gap)

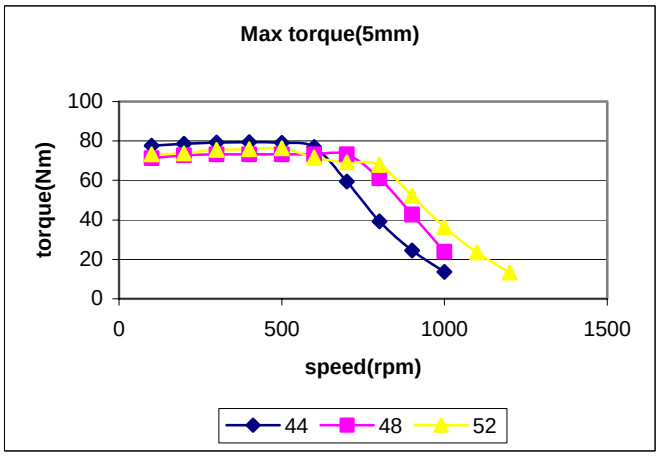

Figure 29: Maximum Torque at Different Input Voltages (5-mm gap)

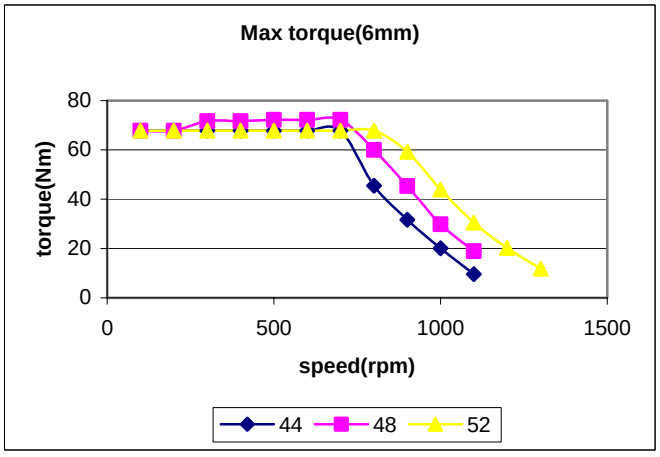

Figure 30: Maximum Torque at Different Input Voltages (6-mm gap)

At each air gap, the maximum torque at the low-speed region is almost the same regardless of input voltage. But as speed increases, the maximum torque also increases as the input voltage is increased.

The efficiencies at different input voltages are shown in Figures 31 and 32. At low torque with low input voltage, the efficiency is slightly higher than the other cases. The efficiencies are almost the same, regardless of input voltage in all other regions.

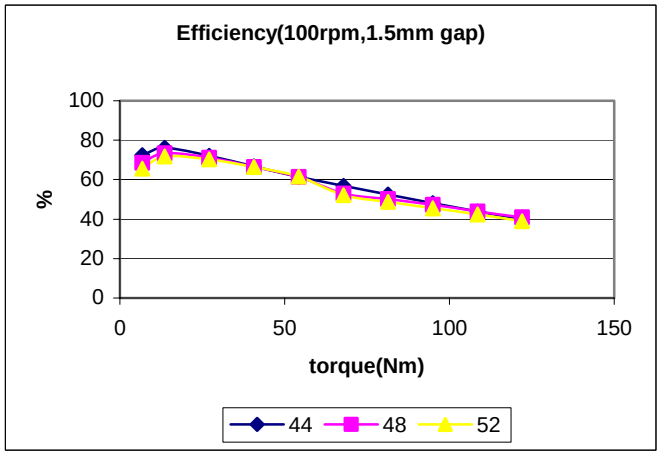

Figure 31: Efficiency at Different Input Voltages (100 rpm, 1.5-mm gap)

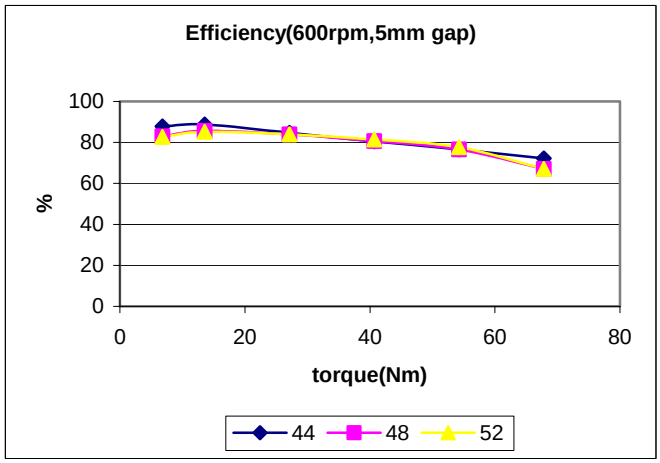

Figure 32: Efficiency at Different Input Voltages (600 rpm, 5-mm gap)

The optimal air gap and corresponding efficiency were also estimated for all four quadrants of operation. Regardless of the input voltage, the distribution of air gap and efficiency are similar to rated voltage operation. The air gap and efficiency distribution for 44-V operation are shown in Figures 33 and 34.

Air gap and efficiency distribution for 52-V operation are shown in Figures 35 and 36.

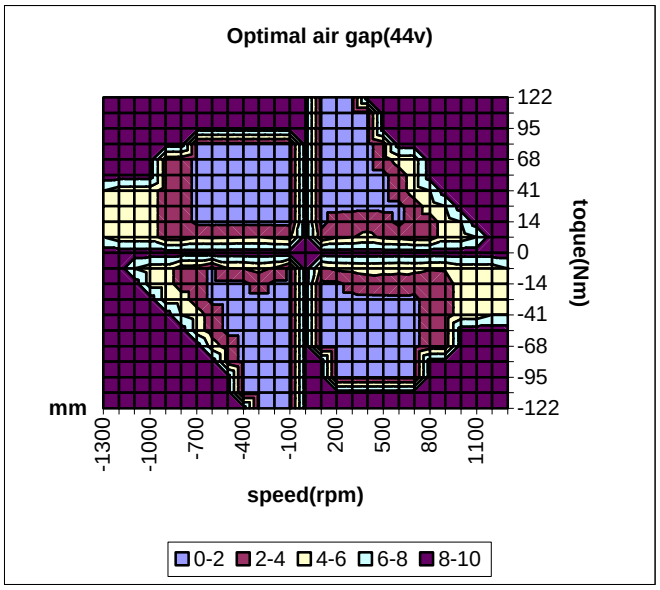

Figure 33: Optimal Air Gap (44-V operation)

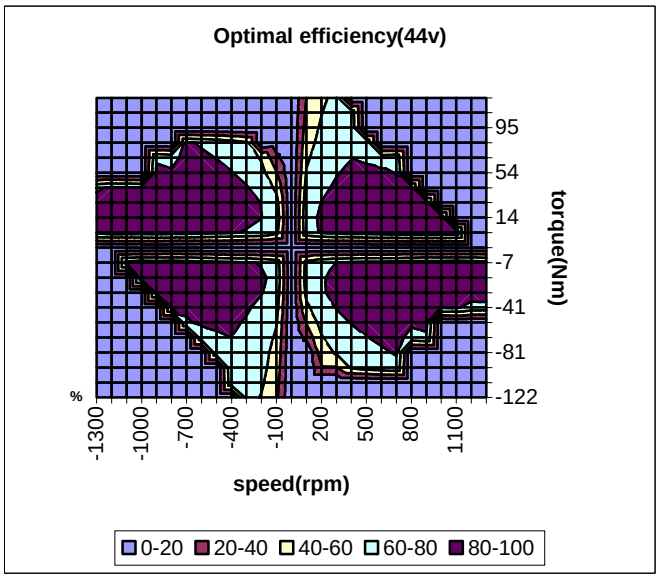

Figure 34: Optimal Efficiency (44-V operation)

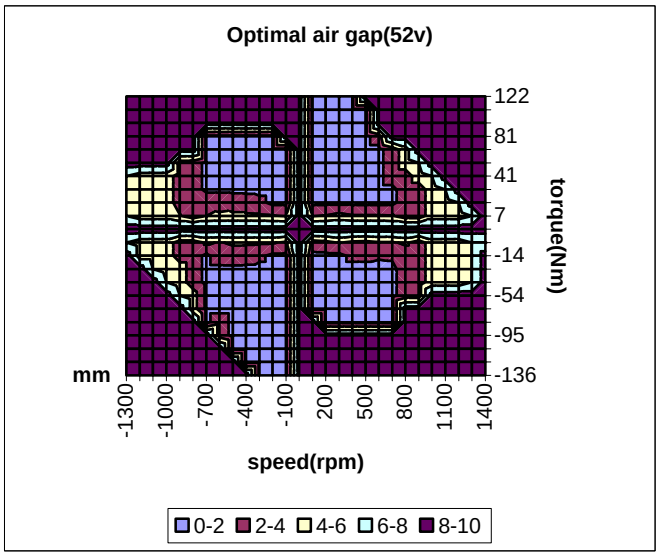

Figure 35: Optimal Air Gap (52-V operation)

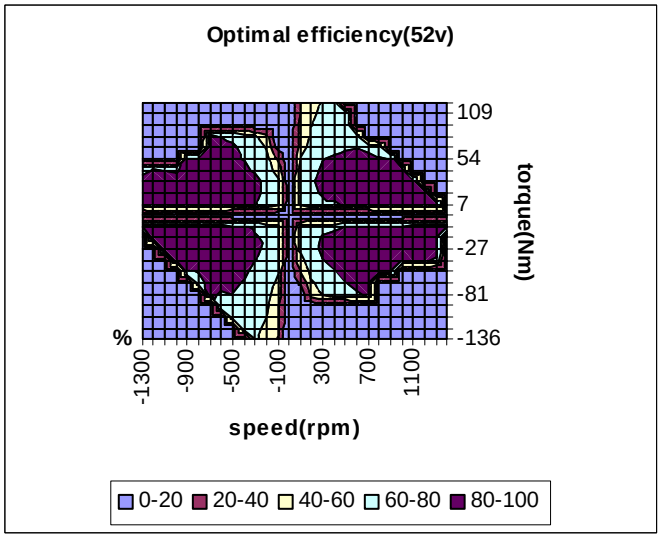

Figure 36: Optimal Efficiency (52-V operation)

PSAT VEHICLE SIMULATION

On the basis of the test results, the performance of a hybrid electric vehicle (HEV) with axial flux motors was analyzed by using PSAT. The vehicle used for the simulation was the default series hybrid configuration with a four-wheel motor topology. Some modifications were made to the motor and controller model in PSAT to simulate the four-wheel motor topology. Table 3 shows the fuel economy of the simulated vehicle and default PSAT series HEV. The results show that the fuel economy of the axial flux motor-driven vehicle is slightly better than that of the default configuration. Table 4 shows the vehicle and motor specifications for each vehicle. More work is needed to optimize the fuel economy of the proposed vehicle.

Table 3: Simulated Fuel Economy

Test Cycle	Induction motor	Axial flux motor
FHDS (mpg)	35.09	38.40
FUDS (mpg)	22.27	23.87

Table 4: Vehicle and Motor Specifications

	Induction motor	Axial flux motor
Vehicle mass (kg)	1814	1798
Cd	0.25	0.25
Frontal area (m^2)	1.8	1.8
Fuel converter (kW)	41	41
Generator unit (kW)	35	35
Drive train	Series with transmission	Series with 4 wheel motors
Motor mass (kg)	115	99 (24.86×4)
Motor peak power (kW)	35	14 (3.5×4)
Motor rotor inertia (kg m^2)	0.1194	0.0782

CONCLUSION

The efficiency of an axial flux motor was measured as a function of motor torque, speed, input voltage, and air gap (in all four quadrants). Based on the efficiency measurements, an optimal air gap to minimize power loss was estimated by interpolation. By changing the air gap during operation, the motor operating range was extended and the efficiency was increased for any given operating point. At a relatively low-torque region, efficiency was improved by increasing the air gap.

Test results were used to develop a PSAT motor and controller model for the axial flux motor. A series HEV equipped with the axial gap motor and new control strategy was simulated, resulting in improved fuel economy. Further improvements could result from directed efforts on a reliable air gap control mechanism. The dynamic response caused by gap variation should be analyzed.

REFERENCES

[1] D. Patterson, “Recent Advances in the Design and Construction of Axial Flux Permanent Magnet Machines,” Proc. of IEEE Aust. Summit, Darwin 1996, pp. 435-440.

[2] D. Patterson and R. Spee, ”The Design and Development of an Axial Flux Permanent Magnet Brushless DC Motor for Wheel Drive in a Solar Powered Vehicle,” IEEE Trans. on IA, Vol 31. No.5, 1995, pp. 1054-1061.

[3] F. Caricchi, F. Crescimbini, F. Capponi and L Solero, “Permanent-Magnet, Direct-Drive, Starter/Alternator Machine with Weakened Flux Linkage for Constant-Power Operation Over Extremely Wide Speed Range,” Proc. of IAS ’01.

[4] B. Conlon, ”A Comparison of Induction, Permanent Magnet, and Switched Reluctance Electric Drive Performance in Automotive Traction Applications,” Advanced Propulsion & Emission Technology, GPC ’01, pp 32-47.

[5] J. Jermakian, M. Mohd, and V. Motevalli, “ Testing and Modeling of Variable Axial Flux Brushless DC Motor,” Argonne National Laboratory, December 2000.

CONTACT

Justin Kern
Center For Transportation Research
Argonne National Laboratory
Phone: (630) 252-6403
E-mail: jkern@anl.gov